HHS Public Access

Author manuscript

Langmuir. Author manuscript; available in PMC 2017 September 27.

Published in final edited form as:

Langmuir. 2016 September 27; 32(38): 9883–9891. doi:10.1021/acs.langmuir.6b02421.

Organization and Structure of Branched Amphipathic Oligopeptide bilayers

Zhiguang Jia, **Susan K Whitaker**, **John M. Tomich**, and **Jianhan Chen***

Department of Biochemistry and Molecular Biophysics, Kansas State University, Manhattan, KS 66506, USA

Abstract

A class of self-assembling Branched Amphiphilic Peptide Capsules (BAPCs) was recently developed that could serve as a new drug delivery vehicle. BAPCs can encapsulate solutes up to ~12 kDa during assembly, are unusually stable and readily taken up by cells with low cytotoxicity. Coarse-grained simulations have supported that BAPCs are defined by bilayers that resemble those formed by diacyl-phospholipids. Here, atomistic simulations were performed to characterize the structure and organization of bilayers formed by three branched amphiphilic peptides (BAPs), bis(Ac-FLIVIGSII)-K-K_4-CO-NH_2, bis(Ac-CHA-LIVIGSII)-K-K_4-CO-NH_2, and bis(Ac-FLIVI)-K-K_4-CO-NH_2, respectively. The results show BAPs form a network of intra- and intermolecular backbone hydrogen bonds within the same leaflet in addition to hydrophobic sidechain interactions. The terminal residues of two leaflets form an interdigitation region locking two leaflets together. The phenyl groups in bis(Ac-FLIVIGSII)-K-K_4-CO-NH_2 and bis(Ac-FLIVI)-K-K_4-CO-NH_2 are tightly packed near the bilayer center, but do not formed ordered structures with specific π-π stacking. Replacing phenyl groups with the cyclo-hexane sidechain only slightly increases the level of disorder in bilayer structures, and thus should not significantly affect the stability, consistent with experimental results on bis(Ac-CHA-LIVIGSII)-K-K_4-CO-NH_2 BAPCs. Self-assembly simulations further suggest that leaflet interdigitation likely occurs at early stages of BAPC formation. Atomistic simulations also reveal that the BAPC bilayers are highly permeable to water. This prediction was validated using fluorescence measurements of encapsulated self-quenching dye upon transferring BAPCs to buffers with different salt concentrations. Improved understanding of the organization and structure of BAPC bilayers at atomic level will provide a basis for future rational modifications of BAP sequence to improve BAPC properties as a new class of delivery vehicle.

INTRODUCTION

The use of drugs in free forms are often limited by unfavorable properties such as low aqueous solubility, poor biodistribution, and high break down rate in vitro or in vivo.[2] In addition, some drugs are toxic or have potential danger of inducing an immune response when administered directly.[3, 4] To compensate for these undesirable properties and improve therapeutic efficiency, association of drugs with appropriate drug carriers is often necessary.[2] However, while tremendous improvements have been made over the years, some important

*Corresponding Author: Phone: (785) 532-2518; Fax: (785) 532-7278; jianhanc@ksu.edu.

limitations remain for the currently available dug carriers.[2, 4] For example, it remains challenging for lipid/polymeric-based vesicles to deliver drugs to specific organs or tissues, and uptake of drugs by off-target organs often leads to side-effects.[3] It also remains difficult for traditional lipid-based carrier to deliver macromolecules such as protein, or highly charged molecules such as oligonucleotides for siRNA and gene therapy.[3, 5, 6] In addition, intracellular degradation products of some polymeric-based carrier can be toxic.[4] As protein drugs and gene therapeutics become increasingly promising tools against diseases such as cancers, heritable genetic disorders, and viral infections, there is a pressing need to develop new drug delivery vehicles and overcome these shortcomings.[3, 5, 7]

Gudlur et al. first described a new peptide-based nano-vesicles, formed from aqueous self-assembly of branched amphiphilic peptides (BAP).[8] The molecular architecture of BAPs was designed to mimic that of diacyl-phospholipids. It contains a poly-lysine head group, analog to the charged phosphate-based head of lipid, and two identical hydrophobic segments connected to α and ε amino groups of the N-terminal lysine residue, respectively. The chemical structure of three BAPs investigated in the current study, bis(Ac-FLIVIGSII)-K-K_4-CO-NH_2, bis(Ac-CHA-LIVIGSII)-K-K_4-CO-NH_2 and bis(Ac-FLIVI)-K-K_4-CO-NH_2 peptides, are showed in Fig. 1. Coarse-grained (CG) simulations have demonstrated that BAPs can self-assemble into bilayers in water, in a manner similar to diacyl-phospholipids.[8, 9] The resulting BAP capsules (BAPCs) have diameters ranging from 20 nm to 2 μm depending on the assembly and annealing temperatures.[11] BAPCs have several attractive properties as a potential delivery vesicle. They can encapsulate macromolecules, up to ~12 kDa proteins and have long intracellular life-time (> 2 weeks) after uptake.[9, 10, 11] BAPCs are extremely stable in water and can maintain their structure to at least 95°C.[9] Although their high stability allow the BAPCs to be used to deliver radioisotopes for cancer therapy, it is difficult to use BAPCs as a general drug delivery system.[10] To design new BAP sequences with higher cargo release rate, improved knowledge of the organization and structure of BAP bilayers is necessary.

Circular dichroism (CD) spectra analysis show that BAPs mainly sample a mixture of β and random coil secondary structures and their conformational states can depend quite sensitively on the temperature of self-assembly and post-assembly annealing process. Specifically, the BAP assembled at 37 °C or 4 °C was found trapped in beta or random coil conformation, respectively.[8, 12] Replacing the terminal PHE residue to cyclohexyl-L-alanine (CHA) lead to a full beta structure throughout the temperature range 4–25 °C.[12] CG simulations have been previously performed to investigate the self-assembly of bis(Ac-FLIVI)-K-K_4-CO-NH_2[8] and a BAPC consisted of bis(Ac-FLIVIGSII)-K-K_4-CO-NH_2 and bis(Ac-CHA-LIVIGSII)-K-K_4-CO-NH_2[9] using the MARTINI force field.[13] The results support that BAPs likely assemble into bilayer structures in BAPCs and the two leaflets have minimal-interdigitation. The coarse-grained simulations could not supply atomic level details of the backbone and sidechain interactions underlying the unusual stabilities of BAPCs. In this study, we exploit long-time molecular dynamics (MD) simulations at atomistic level to examine the structure and organization of bilayers formed by three BAPs: bis(Ac-FLIVIGSII)-K-K_4-CO-NH_2, bis(Ac-CHA-LIVIGSII)-K-K_4-CO-NH_2, and bis(Ac-FLIVI)-K-K_4-CO-NH_2. A particular focus is to understand the nature of molecular

interactions underlying the unusual thermal stability of BAPCs and the possible origins of thermally induced conformation transitions.

METHODS

MD simulations

All simulations were performed using the GROMACS (Groningen Machine for Chemical Simulation) package version 4.0.5[14, 15] in conjunction with the GROMOS 54A7 force field.[16] The solvent water was represented using the simple point charge (SPC) water model[17]. The solvent and solute were coupled independently to an external temperature bath (310 K) with a coupling constant of 0.1 ps using the Berendsen thermostat.[18] Periodic boundary conditions were imposed and the pressure was maintained at 1 bar in the lateral and normal directions by weakly coupling to a semi-isotropic (for the simulations start from preassembled bilayer) or isotropic (for the simulations starting from randomized initial conformations) pressure bath. The isothermal compressibility was 4.5×10^{-5} $bar^{-1}$and the coupling constant was 1 ps. The LINCS algorithm[19] was used to constrain the length of all covalent bonds within the solute and the SETTLE algorithm[20] was used to constrain the geometry of the water molecules. Non-bonded interactions were evaluated using a twin-range method, where interactions within the short-range cutoff of 0.8 nm were calculated every step, and those interactions within the long-range cut off of 1.4 nm were recalculated every 3 steps together with the pair list. To correct for the truncation of electrostatic interactions beyond the long-range cut-off, a reaction-field correction was applied using a relative dielectric permittivity of 78[21]. The mass of hydrogen atoms was increased to 4 a.m.u by transferring mass from the atom to which it was attached, allowing a time step of 4 fs to be used to integrate the equations of motion.

System setup

Three pre-assembled bilayers were generated for each BAP molecules (Fig. 1). For this, the monomers were first constructed in fully extended configurations, and then subjected to three independent 300 ns equilibrium simulations in water at 298 K. Three representative monomer structures were then taken from these simulations for each system that are relative extended as observed in our previous CG simulations of BAPCs.[9] Each of the three selected monomer structures was then replicated on an 8 × 8 grid to generate a bilayer containing 128 BAP molecules. The distances between the BAP molecules in the same leaflet were such that the initial area per peptides was similar to value obtained in our previous CG simulations with the Martini force field (~1.4 nm^2).[9] The system was then solvated in a box of SPC water molecules, and neutralized by adding an appropriate number of counter ions (Na^+ and Cl^-) to a final salt concentration of 150 mM (Table 1). Each system was then minimized for 500 steps using a steepest-descent algorithm, followed by 50 ps of equilibration dynamics at 298 K in which the positions of the heavy atoms of BAP molecules were harmonically restrained using a force constant of 500 $kJ.mol^{-1}.nm^2$. All solvated bilayers were simulated for up to 1.1 μs (see Table 1) with all restrains removed, where the time evolution of the potential energy, area per lipid and hydrogen bonding pattern were monitored. In the third simulation of bis(Ac-FLIVIGSII)-K-K_4-CO-NH_2, defects in upper leaflets were observed during the early stage of the production run and persisted for

the rest of the run. This is consistent with the expectation that the membrane resealing likely requires ms timescale.[22] We repeated the simulation after an additional 80 ps restrained equilibration step at 273 K. No defects were observed in the new production run that followed. In addition to simulations initiated from preassembled bilayers, a separate simulation was performed to probe the self-assembly process at atomistic level. For this, 16 bis(Ac-FLIVI)-K-K_4-CO-NH_2 molecules were randomly placed within a cubic water box of ~10 nm in size. The peptides were initially separated at least 1.0 nm from one and another. The self-assembly simulation was performed for 250 ns (see Table 1).

Simulation Analysis

Unless stated otherwise, the structures of the bilayer were extracted from the last 400 ns trajectories every 0.1 ns for analysis. For analysis of the water residence time and hydrogen bond lifetime, structures extracted at 0.01 ns interval were used. All analyses were performed for three independent simulations and then averaged. The area per peptide was computed as the lateral area of the simulation box divided by the number of peptides per leaflet. The 2D radii of gyration of BAP molecule in the bilayer plane (x-y plane) was calculated as the mass-weighted root-mean-square of the radii components on x-y plane:

$$Rg^2_{(z)} = \sum m_i r_i^2 / M, \quad (1)$$

where r_i is the x-y components of the distance between atom i and the center of mass. The secondary structure was assigned using the STRIDE algorithm.[23] Structure clustering was performed with the GROMOS algorithm[24] based on the mutual backbone root-mean-square distance (RMSD) of the hydrophobic tails with a cutoff of 0.4 nm, 0.4 nm and 0.2 nm for bis(Ac-FLIVIGSII)-K-K_4-CO-NH_2; bis(Ac-CHA-LIVIGSII)-K-K_4-CO-NH_2 and bis(Ac-FLIVI)-K-K_4-CO-NH_2, respectively.

The orientation of hydrophobic segments was characterized using the second-rank order parameter, defined as

$$P_2 = \frac{1}{2}(3<\cos^2\theta> - 1) \quad (2)$$

with θ being the angle between the bilayer normal and the vector from the carbonyl C to amide N of a specific residue. The square brackets denote ensemble average. The cases of perfect parallel alignment, perfect anti-parallel alignment, and completely random orientation with respected to the bilayer normal yield $P_2 = 1$, −0.5 and 0, respectively. To quantities the level of order in the packing of the side chain phenyl group of PHE in bis(Ac-FLIVIGSII)-K-K_4-CO-NH_2 and bis(Ac-FLIVI)-K-K_4-CO-NH_2, a general order parameter was calculated as

$$S = \frac{4\pi}{5} \sum |<Y_2^m(\theta, \phi)>|^2, \quad (3)$$

where Y_2^m is a second-rank spherical harmonics and (θ, Φ) are the spherical polar coordinates of the unit vector normal to the phenyl ring. S reflects the degree of alignment along a common vector, and has a value of 1.0 for fully aligned system and 0 for fully random systems.

Peptide synthesis, BAPC formation and Eosin Y self-quenching

Both peptides bis(Ac-FLIVIGSII)-K-K_4 and bis(Ac-FLIVI)-K-K_4 were synthesized as described previously[8,9,11] using solid phase peptide chemistry. They were dissolved individually into 2,2,2-trifluoroethanol and absorbance of phenylalanine was taken to determine the concentration. In preparation for the formation of BAPCs, the peptides were combined in concentrations of 1 mM of each peptide and dried to remove the solvent. The dried peptides were hydrated in a drop-wise fashion with 2.126 mM Eosin Y (Sigma-Aldrich, St. Louis, MO) final concentration at room temperature in distilled, deionized water with 20, 50, 100 or 300 mM NaCl. After sitting for 30 minutes at room temperature, each solution was filtered through a 0.2 μm syringe-driven PTFE filter (EMD Millipore, Billerica, MA) and into Amicon Ultra−0.5 mL centrifugal cellulose filters with a 30 kDa molecular weight cut off (EMD Millipore, Billerica, MA). BAPCs were centrifuged at 14,000 × g using an Eppendorf 5415 D benchtop centrifuge to remove external dye from the BAPCs. Wash steps were performed using the same concentration of NaCl with which the BAPCs were formed, and they were centrifuged at 14,000 × g; wash and the centrifugation steps repeated until the externally bound dye was removed from the outer surface of the BAPCs. The filters were then inverted into clean collection tubes and centrifuged at 2,000 × g to collect the washed BAPCs.

The harvested BAPCs from each salt concentration were then divided into two equal volumes for analysis. One half was brought up to a final concentration of 1 mM BAPCs in the equimolar salt solution in which they were prepared and washed. The other half was diluted to the same concentration in distilled, deionized water. The distilled, deionized water containing BAPCs were diluted as discussed previously in water and in 1 M NaCl. Fluorescence intensities for the encapsulated Eosin Y were measured using a CARY Eclipse fluorescence spectrophotometer (Varian Inc., Palo Alto, CA) immediately upon dilution using an excitation wavelength at 500 nm and observing the fluorescence from 505 to 800 nm within a 0.3 cm path length quartz cuvette. (scan rate: 600 nm/min; PMT detector voltage: 600 V; excitation slit: 5 nm; emission slit: 5 nm).

RESULTS AND DISCUSSION

Structural characteristics of BAP Bilayers

All three BAPs can maintain stable bilayer structures in all simulations starting from different initial conformations with proper equilibration. Key structural properties, e.g., bilayer thickness, number of hydrogen bonds and area per peptides, were monitored during simulations to examine the level of convergence. As illustrated in Fig. S1, virtually all structural properties reached plateau within ~300 ns and remain stable for the rest of simulations. As such, all analysis were performed using the last 400 ns of the trajectories. Key properties of the BAP bilayers are summarized in Table 2. As illustrated in Fig. 2, the

overall organization of BAP bilayers are very similar to those formed by phospholipids. The charged C-terminal poly-lysine “head groups” (blue) project towards bulk water, while the branched N-terminal hydrophobic residues (brown) pack together and form a hydrophobic core. For bis(Ac-FLIVIGSII)-K-K_4-CO-NH_2 and bis(Ac-CHA-LIVIGSII)-K-K_4-CO-NH_2, the hydrophilic residues (green) form an additional layer between the charged LYS residues and the hydrophobic layer. The average area per peptide is slightly larger (~1.5 nm^2) for the BAPs with longer hydrophobic segments (bis(Ac-FLIVIGSII)-K-K_4-CO-NH_2 and bis(Ac-CHA-LIVIGSII)-K-K_4-CO-NH_2) than the 1.3 nm^2 observed with shorter hydrophobic segments (bis(Ac-FLIVI)-K-K_4-CO-NH_2 (Table 2). The BAPs with longer tails also have larger 2D radii of gyration and forms more tightly packed membranes than those with shorter hydrophobic branches (Table 2). Fig. 3 shows the average electron density profiles of different components. The thickness of the bilayers, defined as the distance between the peaks of poly-lysine electron density profiles from the top and bottom leaflets (red traces in Fig. 3), was ~6 nm for bis(Ac-FLIVIGSII)-K-K_4-CO-$NH_2$and bis(Ac-CHA-LIVIGSII)-K-K_4-CO-NH_2 and ~5 nm for bis(Ac-FLIVI)-K-K_4-CO-NH_2. With all residues included, the electron density profile of either the top or the bottom leaflet (green traces in Fig. 3) crosses the bilayer mid-planes and penetrates into the other leaflet. The thickness of interdigitating regions was ~2 nm, which is larger than those observed in phospholipid bilayer.[25]

Networks of hydrophobic and hydrogen-bonding interactions

A key objective of atomistic simulations has been to characterize the interactions among BAPs that give rise to the unusual stability of BAPCs. The substantial interdigitation in BAP bilayers appears to allow extensive interactions between the hydrophobic segments from two leaflets. As shown in Fig. 3, interdigitated regions mainly include the N-terminal PHE1/CHA1 and LEU2 residues (blue and purple traces). In particular, the last PHE/CHA1 residue appears to play a dominant role in the inter-leaflet interactions, contributing over 80% of the penetrating part of the electron density profile. It was previously speculated that the aromatic sidechains of PHE residues could form ordered structures with specific π-π stacking as previously observed in peptide nanostructures[26]. However, the current simulations suggest that the phenyl rings bis(Ac-FLIVIGSII)-K-K_4-CO-NH_2 and bis(Ac-FLIVI)-K-K_4-CO-NH_2 bilayers are completely disordered, yielding diminishing general order parameters in both cases (see Table 2). The prediction that the aromatic nature of PHE sidechains is not likely a key factor for the unusual stability of BAPCs is consistent with a previous study showing that replacing PHE with CHA does not significantly destabilized the BAPCS.[12] As shown in Fig. 3B, PHE to CHA mutation does not reduce the level of leaflet interdigitation (Fig. 2B, blue and purple trace). As detailed below, the substitution does slightly increases the level of disorder of BAP peptides in the bilayer and results modest reduction in packing density and number of intra- and inter-molecular interactions. The implication is that the bis(Ac-CHA-LIVIGSII)-K-K_4 bilayer should have slightly reduced (thermo-)stability, which appears fully consistent with the previous experimental studies.[12]

The interdigitation between leaflets allows extensive nonpolar interactions within and between leaflets, not only between terminal residues (PHE1 and LEU2) but also involving central hydrophobic residues (ILE3, VAL4 and ILE5). In particular, as illustrated in Fig. S2, hydrophobic residues (ILE3: green; VAL4: orange and ILE5: brown) from the top leaflet can

make close contacts with PHE1 from the bottom leaflet. Fig. S3 shows the distribution of minimum distances between PHE1 sidechains from one leaflet and to side chains of ILE3 (solid line), VAL4 (dash line) and ILE5 (dot line) from the other leaflet. These distributions clearly show peaks between 0.3–0.5 nm, which indicate the existence of close contacts. The population of PHE1/CHA1 involved in the interactions with these residues (minimum distance < 0.5 nm) were similar in bis(Ac-FLIVIGSII)-K-K_4-CO-NH_2 (36%, 19% and 12% for ILE3, VAL4 and ILE5, respectively) and bis(Ac-CHA-LIVIGSII)-K-K_4-CO-NH_2 (39%, 15% and 10% for ILE3, VAL4 and ILE5, respectively). In bis(Ac-FLIVI)-K-K_4-CO-NH_2, the population of PHE1 involved in the cross-leaflets interactions is lower than the other two system (21%, 3% and 3% for ILE3, VAL4 and ILE5, respectively), suggesting the packing of bis(Ac-FLIVI)-K-K_4-CO-NH_2 decreases the penetration of PHE1 into the opposite leaflet. The degree of interdigitation can be correlated with the strength of coupling between leaflets for phospholipid bilayers.[25] It is likely that substantial interdigitation in BAP bilayers, and thus stronger cross leaflet hydrophobic interactions, is a key reason for the unusual stability of BAPCs.

Besides extensive hydrophobic interactions, BAP bilayers also support extensive backbone hydrogen bonding interactions within and across leaflets that are completely absent in traditional phospholipid bilayers. On average, BAP molecules make 3.3 to 4.3 inter-molecular hydrogen bonds, in addition to 4.4 to 6.7 intra-molecular ones (i.e., between two hydrophobic branches) (see Table 2). Interdigitation also allows substantial cross-leaflet hydrogen bonding interactions. The average number of cross-leaflet hydrogen bonds for each BAP molecule ranges from 0.7 to 1.8 for the three systems (Table 2). Importantly, the peptides do not appear to form stable and persisting β-sheets. The average lifetimes of these backbone hydrogen bonds are short, ranging only from 34 to 70 ps. The highly dynamic nature of the hydrogen-bonding network within the bilayers appears consistent with the ability of BAPCs to fuse or resized when assembled at the room temperature. Nonetheless, the ability to form extensive hydrogen bonding network through the peptide backbone is clearly another key factor that contributes to BAPC stabilities. The ability to form hydrogen bonding networks also greatly reduces the lateral diffusion constant of BAP molecules within the bilayers, which is about 1% of that of lipid molecules in more fluid phase membranes (Table 2).[27]

Conformational properties of BAPs in the bilayer

While the charged poly-lysine tails are highly disordered and well hydrated, the hydrophobic segments adopt more ordered structures to support extensive intra- and inter-molecular hydrogen bonding interactions (Fig. 2). To examine the conformation of hydrophobic segment, cluster analysis based on the mutual backbone RMSD was performed. The centroid structures of the first 5 clusters are showed in Fig. 4. The first cluster accounts for approximately 60%–69% of the ensemble, where both hydrophobic segments are relatively extended conformation. For bis(Ac-FLIVIGSII)-K-K_4-CO-NH_2 and bis(Ac-CHA-LIVIGSII)-K-K_4-CO-NH_2, hydrophobic segments can be substantially disordered in clusters 2–5, which together account for ~25% of the population. In shorter bis(Ac-FLIVI)-K-K_4-CO-NH_2, the hydrophobic segments adopt the extended structure in the top 4 clusters. Interestingly, the longer BAP peptides with more disordered conformations also have shorter

hydrogen bond life time (~50 ps) compared to the shorter bis(Ac-FLIVI)-K-K_4-CO-NH_2 peptides (~70 ps) (see Table 2). A reduced intra-hydrogen bond lifetime was also observed in more disordered CHA-mutation bilayers (~50 ps to ~30 ps).

The average secondary structure of BAP was calculated from last 400 ns of simulations. The results, summarized in Fig. 5, show that BAPs mainly sample beta and coil-like secondary structures in the bilayer. This is consistent with previous CD studies on BAPCs freshly assembled at the room temperature.[12] Replacing PHE with CHA leads to substantial decrease in the level of β secondary structure in the hydrophobic segment, even though the average numbers of intra and inter-peptide hydrogen bonds remain very similar (see Table 2). For bis(Ac-FLIVIGSII)-K-K_4-CO-NH_2 and bis(Ac-CHA-LIVIGSII)-K-K_4-CO-NH_2, transient helices involving SER7 to ILE9 (on the main branch) and poly-lysine residues have been observed in the bilayers. This appears to reflect an intrinsic conformational tendency of BAPs. Similar helical propensities can be observed BAP monomers in water (Fig. S4), even though the random coil propensity is higher compared to when incorporated into bilayers. In Fig. 6, we further examine the ordering of BAP peptides with respect to the bilayer normal, as quantified by the second rank order parameter P_2 as a function of residue number. The results correlate well with the peptide secondary structures discussed above. All three BAPs bilayer had similar, diminishing order parameters in the poly-lysine head group region, but demonstrate varied levels of ordering in the hydrophobic branches. The shorter BAP, bis(Ac-FLIVI)-K-K_4-CO-NH_2, prefers more extended structures (Fig. 4) and has the most ordered hydrophobic region among all three sequences.

Peptide-water interactions in BAP bilayers

Another distinct property of BAP bilayers involves the extent and nature of peptide-water interactions. In phospholipid bilayers, there is essentially no water density in the hydrophobic center[28]. For BAP bilayers, the water density drops from ~320 e.nm^{-3} (bulk water region) to ~40 e.nm^{-3} after crossing the poly-lysine head region, but remains non-diminishing throughout the BAP bilayers, with the lowest water electron density of ~3–5 e.nm^{-3} near the bilayer center (see Fig. 3, black traces and Table 2). The average electron density of water in the hydrophobic core region was 4–8 e.nm^{-3}. As a result, each BAP molecule can form ~3–10 water-backbone hydrogen bond interactions in the hydrophobic region (Table 2). Importantly, water molecules in the hydrophobic regions of BAP bilayers are highly dynamic. The average water residence time within the bilayer hydrophobic core is only ~0.2 ns, with only a few “structural” water molecules that have long residence times up to ~40 ns. The average rate of water transport is ~0.03 $nm^{-1}.ns^{-1}$ for BAP bilayers with longer hydrophobic segments and ~0.06 $nm^{-1}.ns^{-1}$ for the BAP bilayer with short hydrophobic segments. The average time for a single water molecule to cross the bilayer core is 9–17 ns (Table 2). Fig. S5 shows a typical trajectory of water diffusion spontaneously through the BAP bilayer. Note that, although water can penetrate easily into the BAP bilayer, no density of ions was observed in the bilayer core, suggesting that ions could not permeate spontaneously through BAP bilayers. Water permeability may also contribute to the unusual stability of BAPCs, allowing BAPCs to expand or contract in response to changing external osmotic pressure.

Change of BAPC internal solute concentration in response to salt gradient

To test if water can permeate readily through BAP bilayers while the ions cannot, we examined the effects of osmotic pressure on the internal solute concentration when BAPCs were placed in external solutions with different salt concentrations. This was achieved by measuring the fluorescence intensity of self-quenching dye Eosin Y encapsulated in BAPCs (see Fig. S6).[11] If the BAP bilayer is semi-permeable to water, the flux of water into or out of the dye-filled capsules will change the internal Eosin Y concentration and lead to changes in the fluorescence intensity. To normalize for batch to batch variations with Eosin Y encapsulation from different experiments, we only examine the relative fluorescence intensity change when diluted in hyper- or hypo-tonic solutions with respect to the reference BAPCs that were diluted into isotonic solutions (see Methods for details). The measured fluorescence intensity was further corrected to account for different fluorescence properties of Eosin Y dye in water versus NaCl solutions.

The results, summarized in Fig. 7, clearly support the prediction that BAP bilayers are permeable to water but not to ions. Exposure of water-filled BAPCs (that is, zero internal NaCl concentration) to 1.0 M NaCl buffer leads to ~14% decrease in internal Eosin Y fluorescence intensity (left most bar), suggesting a net out flux of water and thus increase in internal Eosin Y concentration. In contrast, when BAPCs prepared with different internal NaCl concentrations were placed in pure water, there were net increases in the Eosin Y fluorescence intensities (right four bars of Fig. 7). The degree of fluorescence intensity increase clearly correlates with the NaCl concentration difference across the BAP bilayer. Assuming that there is minimal ion movement across BAP bilayers, we can further quantify the Eosin Y concentration changes using a standard curve of fluorescence intensity. The results are summarized in Fig. S6. Exposing BAPCs with initial NaCl concentration of 300 mM to pure water dilutes the internal Eosin Y concentration to approximately 500 μM, compared to the initial concentration of 2130 μM where the BAPCs were formed. In contrast, exposing BAPCs with no internal salt to 1.0 M NaCl buffer approximately double the internal Eosin Y concentration. We note that all BAPCs were filled with the same concentration of Eosin Y dye, fusion between BAPCs should not lead to any change in fluorescence. Together, these experiments reveal a surprising level of plasticity associated with BAP bilayers under osmotic pressure. The structural basis of such plasticity is not obvious from the current simulations and will be further investigated in future studies.

Early stages of aggregation and self-assembly of BAPs

Besides simulations initiated from preformed bilayers, a separate simulation was performed examine the early stages of BAP aggregation and self-assembly at atomistic level. The simulation was initiated from 16 bis(Ac-FLIVI)-K-K_4-CO-NH_2 peptides randomly placed as monomers in a water box. As shown in Fig. 8, small clusters emerged quickly, within 50 ns (Fig. 8B), which merged into a single cluster by 250 ns (Fig. 8C–D). The large cluster has a connected hydrophobic core region (Fig. 8D, brown) with the LYS residues projecting outward (Fig. 8, D, blue). In the initial cluster, the terminal PHE1 residue (van der Waals surface) tended to stack together (Fig. 8B–C), thereby restricting the relative orientation of neighboring BAP peptides. As a result, the peptides tend to adopt parallel orientation or tail-to-tail orientation. For example, Fig. 8E shows the snapshot of a cluster contain 6 BAP

molecules observed at ~80 ns, in which all peptides has a neighbor peptide adopted either parallel or tail-to-tail orientation.

We note that another vesicle-forming peptide, Self-Assembling peptide 2 (SA2 peptide, Ac-AAVVLLLWEE-COOH) were recently shown to adopt antiparallel and interdigitated structures.[29] Increasing the GLU residues at the C-terminus of SA2 from 2 to 7 did not change the overall structure of SA2 vesicle.[30, 31] Thus, the difference in the peptide orientation in SA2 and BAP assemblies is not likely due to different head-tail ratios and are more likely a result of the peptide sequences.[30] As showed in the self-assembly simulation of BAP, the PHE/CHA clusters formed during the early stages of aggregation, would make a parallel/tail-to-tail orientation more favored. As the PHE cluster kept growing during the assembling of small clusters, the preference of parallel orientation is preserved in the final vesicle structure.

CONCLUSION

Long-timescale atomistic simulations have been performed to analyze the structure and interactions of three different BAP bilayers. The results support that the overall structure of BAP bilayers is similar to those formed by phospholipids. However, BAP bilayers contain extensive networks of intra- and inter-molecular backbone hydrogen bonding interactions. BAP bilayers also possess larger degree of interdigitation between the top and bottom leaflets. The interdigitation region is dominated by the interactions between last two residues, which forms early in the assembly process and plays an important role in the ultimate peptides alignment as well as maintaining bilayer stability. In addition, water was found able to readily permeate through the BAP bilayers while ions cannot, a prediction that has been subsequently validated by fluorescence measurements of encapsulated self-quenching Eosin Y. Together, the current atomistic simulations and experiment yield important new details on the molecular interactions underlying the unusual stability of BAPCs and provides a foundation for future efforts that aim to rationally modify the BAP sequence to improve the properties of BAPCs as a new class of delivery vehicle.

Supplementary Material

Refer to Web version on PubMed Central for supplementary material.

Acknowledgments

This work was supported by the National Science Foundation (CHE 1265850 to J.C.) and National Institute of Health (GM114300 to J. C.). Part of the computing for this project was performed on the Beocat Research Cluster at Kansas State University. Computer resources was also used at Extreme Science and Engineering Discovery Environment (XSEDE) facilities (TG-MCB140210). This work is contribution number 16-324-J from the Kansas Agricultural Experiment Station.

REFERENCES

1. Barros SM, Whitaker SK, Sukthankar P, Avila LA, Gudlur S, Warner M, Beltrão EIC, Tomich JM. A review of solute encapsulating nanoparticles used as delivery systems with emphasis on branched amphipathic peptide capsules. Archives of Biochemistry and Biophysics. 2016; 596:22–42. [PubMed: 26926258]

2. Allen TM, Cullis PR. Drug delivery systems: Entering the mainstream. Science. 2004; 303(5665): 1818–1822. [PubMed: 15031496]

3. Torchilin VP, Lukyanov AN. Peptide and protein drug delivery to and into tumors: challenges and solutions. Drug Discovery Today. 2003; 8(6):259–266. [PubMed: 12623240]

4. Muller RH, Keck CM. Challenges and solutions for the delivery of biotech drugs – a review of drug nanocrystal technology and lipid nanoparticles. Journal of Biotechnology. 2004; 113(1–3):151–170. [PubMed: 15380654]

5. Reischl D, Zimmer A. Drug delivery of siRNA therapeutics: potentials and limits of nanosystems. Nanomedicine: Nanotechnology, Biology and Medicine. 2009; 5(1):8–20.

6. Torchilin VP. Recent approaches to intracellular delivery of drugs and DNA and organelle targeting. Annual Review of Biomedical Engineering. 2006; 8(1):343–375.

7. Frokjaer S, Otzen DE. Protein drug stability: a formulation challenge. Nat Rev Drug Discov. 2005; 4(4):298–306. [PubMed: 15803194]

8. Gudlur S, Sukthankar P, Gao J, Avila LA, Hiromasa Y, Chen J, Iwamoto T, Tomich JM. Peptide nanovesicles formed by the self-assembly of branched amphiphilic peptides. PLoS ONE. 2012; 7(9):e45374. [PubMed: 23028970]

9. Sukthankar P, Gudlur S, Avila LA, Whitaker SK, Katz BB, Hiromasa Y, Gao J, Thapa P, Moore D, Iwamoto T, Chen J, Tomich JM. Branched oligopeptides form nanocapsules with lipid vesicle characteristics. Langmuir. 2013; 29(47):14648–14654. [PubMed: 24188529]

10. Sukthankar P, Avila LA, Whitaker SK, Iwamoto T, Morgenstern A, Apostolidis C, Liu K, Hanzlik RP, Dadachova E, Tomich JM. Branched amphiphilic peptide capsules: Cellular uptake and retention of encapsulated solutes. Biochimica et Biophysica Acta (BBA) - Biomembranes. 2014; 1838(9):2296–2305. [PubMed: 24565797]

11. Avila LA, Aps LRMM, Sukthankar P, Ploscariu N, Gudlur S, Šimo L, Szoszkiewicz R, Park Y, Lee SY, Iwamoto T, Ferreira LCS, Tomich JM. Branched Amphiphilic Cationic oligopeptides form peptiplexes with DNA: A study of their biophysical properties and transfection efficiency. Molecular Pharmaceutics. 2015; 12(3):706–715. [PubMed: 25647162]

12. Sukthankar P, Whitaker SK, Garcia M, Herrera A, Boatwright M, Prakash O, Tomich JM. Thermally induced conformational transitions in nascent Branched Amphiphilic Peptide Capsules. Langmuir. 2015; 31(10):2946–2955. [PubMed: 25719598]

13. Monticelli L, Kandasamy SK, Periole X, Larson RG, Tieleman DP, Marrink SJ. The MARTINI coarse-grained force field: Extension to proteins. Journal of Chemical Theory and Computation. 2008; 4(5):819–834. [PubMed: 26621095]

14. Hess B, Kutzner C, van der Spoel D, Lindahl E. GROMACS 4: algorithms for highly efficient, load-balanced, and scalable molecular simulation. Journal of Chemical Theory and Computation. 2008; 4(3):435–447. [PubMed: 26620784]

15. van der Spoel D, Lindahl E, Hess B, Groenhof G, Mark AE, Berendsen HJC. GROMACS: fast, flexible, and free. Journal of computational chemistry. 2005; 26(16):1701–1718. [PubMed: 16211538]

16. Schmid N, Eichenberger AP, Choutko A, Riniker S, Winger M, Mark AE, van Gunsteren WF. Definition and testing of the GROMOS force-field versions 54A7 and 54B7. European Biophysics Journal. 2011; 40(7):843–856. [PubMed: 21533652]

17. Berendsen, HJC.; Postma, JPM.; van Gunsteren, WF.; Hermans, J. Interaction models for water in relation to protein hydration. In: Pullman, B., editor. Intermolecular Forces. Reidel Dordrecht; 1981. p. 331-342.

18. Berendsen HJC, Postma JPM, van Gunsteren WF, DiNola A, Haak JR. Molecular dynamics with coupling to an external bath. The Journal of Chemical Physics. 1984; 81:3684.

19. Hess B, Bekker H, Berendsen HJC, Fraaije JGEM. LINCS: a linear constraint solver for molecular simulations. Journal of Computational Chemistry. 1997; 18(12):1463–1472.

20. Miyamoto S, Kollman PA. SETTLE: an analytical version of the SHAKE and RATTLE algorithm for rigid water models. Journal of Computational Chemistry. 1992; 13(8):952–962.

21. Tironi IG, Sperb R, Smith PE, van Gunsteren WF. A generalized reaction field method for molecular dynamics simulations. The Journal of Chemical Physics. 1995; 102:5451.

22. Hibino M, Itoh H, Kinosita K. Time courses of cell electroporation as revealed by submicrosecond imaging of transmembrane potential. Biophysical Journal. 1993; 64(6):1789–1800. [PubMed: 8369408]

23. Frishman D, Argos P. Knowledge-based protein secondary structure assignment. Proteins: Structure, Function, and Bioinformatics. 1995; 23(4):566–579.

24. Daura X, Antes I, van Gunsteren WF, Thiel W, Mark AE. The effect of motional averaging on the calculation of NMR-derived structural properties. Proteins: Structure, Function, and Bioinformatics. 1999; 36(4):542–555.

25. Chiantia S, London E. Acyl chain length and saturation modulate interleaflet coupling in asymmetric bilayers: Effects on dynamics and structural order. Biophysical Journal. 2012; 103(11):2311–2319. [PubMed: 23283230]

26. Sukthankar P, Gudlur S, Avila LA, Whitaker SK, Katz BB, Hiromasa Y, Gao J, Thapa P, Moore D, Iwamoto T, Chen J, Tomich JM. Branched oligopeptides form nanocapsules with lipid vesicle characteristics. Langmuir. 2013; 29(47):14648–14654. [PubMed: 24188529]

27. Poger D, Mark AE. Lipid bilayers: The effect of force field on ordering and dynamics. Journal of Chemical Theory and Computation. 2012; 8(11):4807–4817. [PubMed: 26605633]

28. Poger D, van Gunsteren WF, Mark AE. A new force field for simulating phosphatidylcholine bilayers. Journal of Computational Chemistry. 2010; 31(6):1117–1125. [PubMed: 19827145]

29. Rad-Malekshahi M, Visscher KM, Rodrigues JPGLM, de Vries R, Hennink WE, Baldus M, Bonvin AMJJ, Mastrobattista E, Weingarth M. The supramolecular organization of a peptide-based nanocarrier at high molecular detail. Journal of the American Chemical Society. 2015; 137(24):7775–7784. [PubMed: 26022089]

30. Rad-Malekshahi M, Lempsink L, Amidi M, Hennink WE, Mastrobattista E. Biomedical applications of self-assembling peptides. Bioconjugate Chemistry. 2016; 27(1):3–18. [PubMed: 26473310]

31. van Hell AJ, Costa CICA, Flesch FM, Sutter M, Jiskoot W, Crommelin DJA, Hennink WE, Mastrobattista E. Self-Assembly of recombinant amphiphilic oligopeptides into vesicles. Biomacromolecules. 2007; 8(9):2753–2761. [PubMed: 17696394]

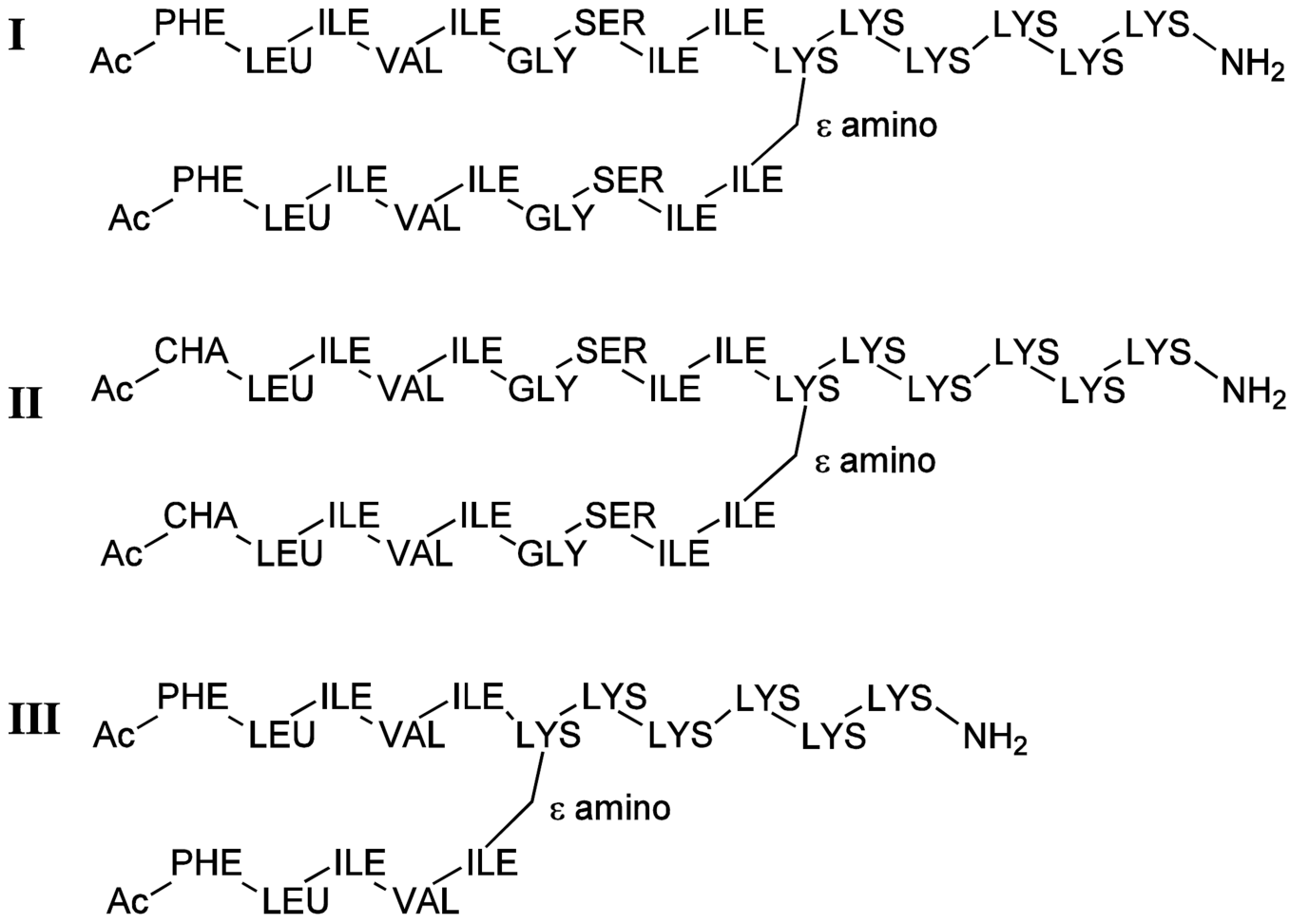

Figure 1.
Schematic representations of three BAPs involved in this study.

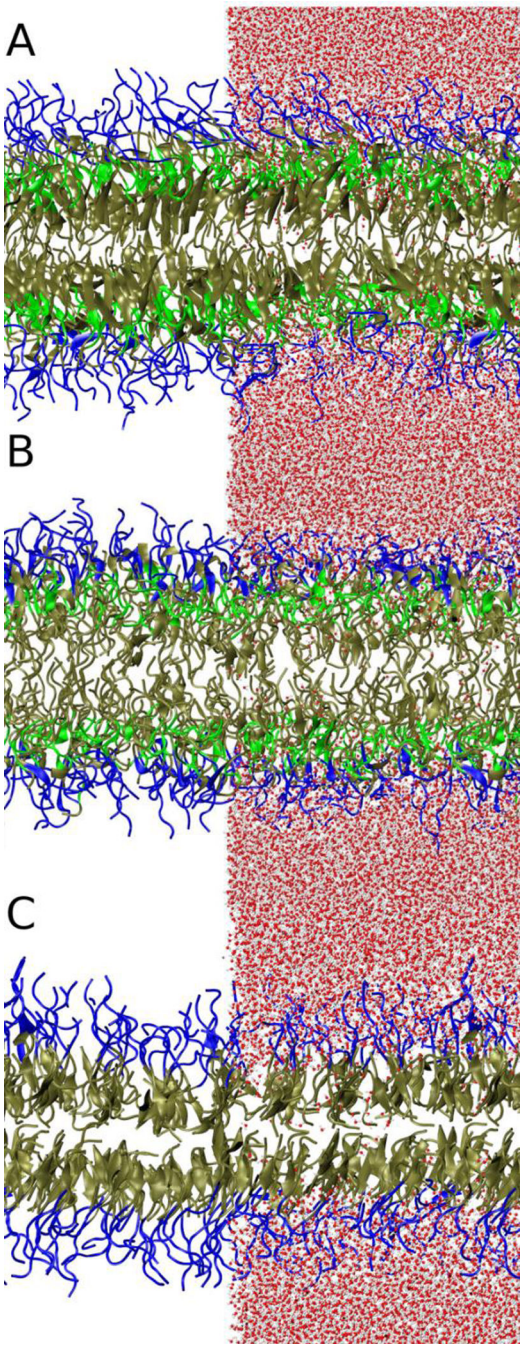

Figure 2.

Representative structures of BAP bilayers, given as the last snapshot of simulation 1 for each system. A: bis(Ac-FLIVIGSII)-K-K_4-CO-NH_2 (1.1 μs); B: bis(Ac-CHA-LIVIGSII)-K-K_4-CO-NH_2 (1.0 μs), and C: bis(Ac-FLIVI)-K-K_4-CO-NH_2 (1.0 μs). BAP molecules are shown in cartoon representations and colored according to the residue types (positive: blue; hydrophilic: green; hydrophobic: brown). Water molecules, represented as balls-and-sticks and colored according to atom type (O, red; H, white), are shown only for the right half for clarity.

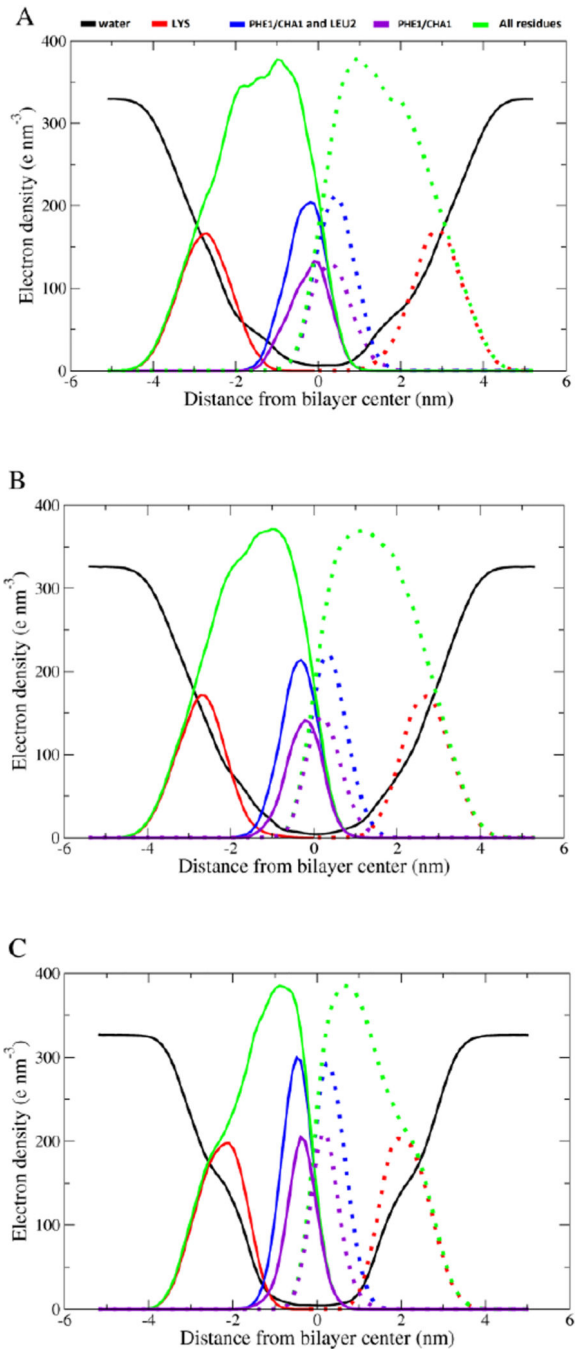

Figure 3.

Electron density profiles of different components along the bilayer normal calculated from the last 400 ns of simulation trajectories. A: bis(Ac-FLIVIGSII)-K-K_4-CO-NH_2; B: bis(Ac-CHA-LIVIGSII)-K-K_4-CO-NH_2 and C: bis(Ac-FLIVI)-K-K_4-CO-NH_2. The electron density profiles for residues in the top and bottom leaflets are showed in solid and dot traces, respectively.

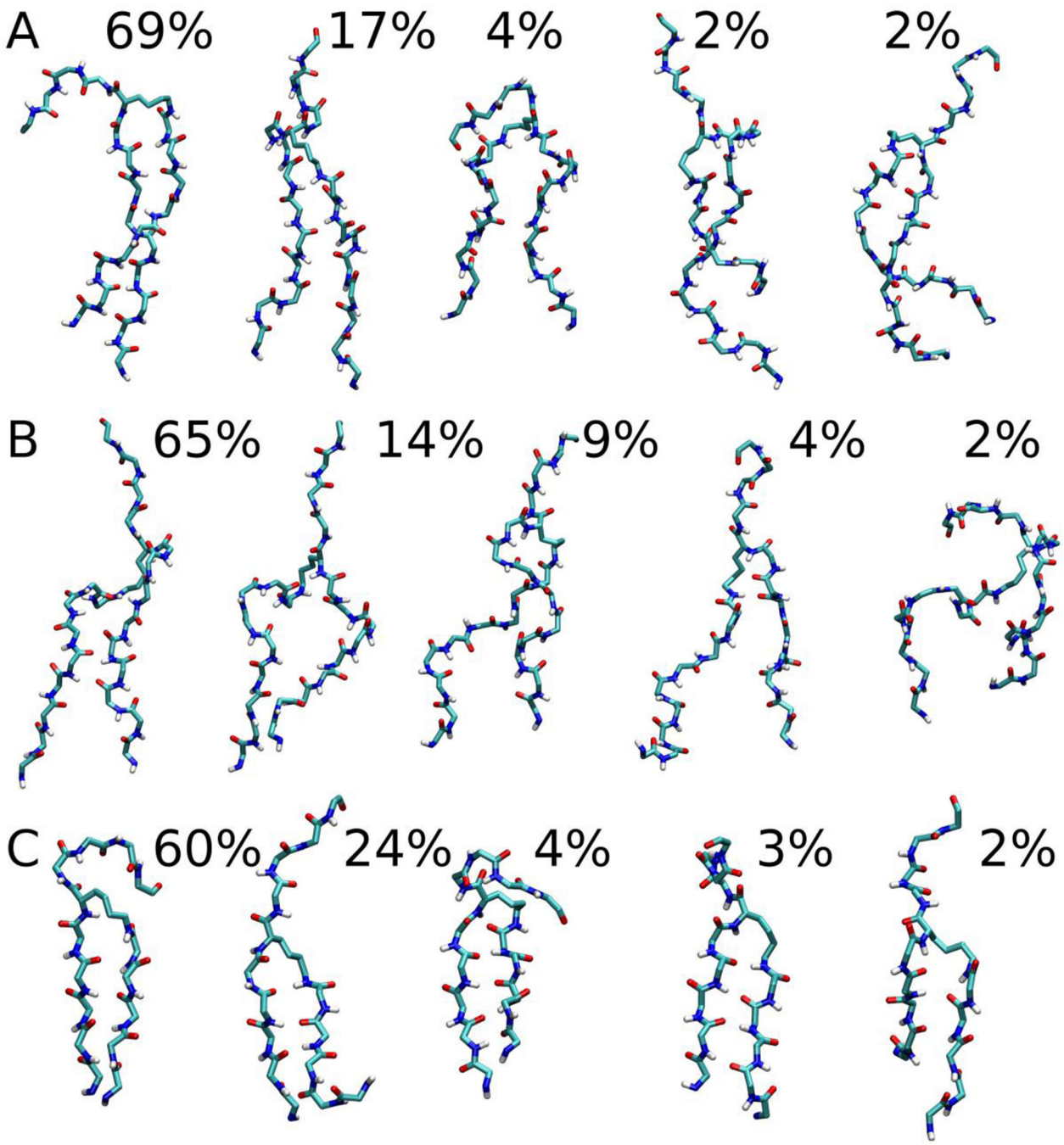

Figure 4.

Centroid structures of the 5 most populated clusters of BAP conformations in bilayers. A: bis(Ac-FLIVIGSII)-K-K_4-CO-NH_2; B: bis(Ac-CHA-LIVIGSII)-K-K_4-CO-NH_2, and C: bis(Ac-FLIVI)-K-K_4-CO-NH_2. The clustering was performed based on mutual backbone RMSD of the hydrophobic tails with a cutoff of 0.4 nm, 0.4 nm and 0.2 nm for the above three systems, respectively.

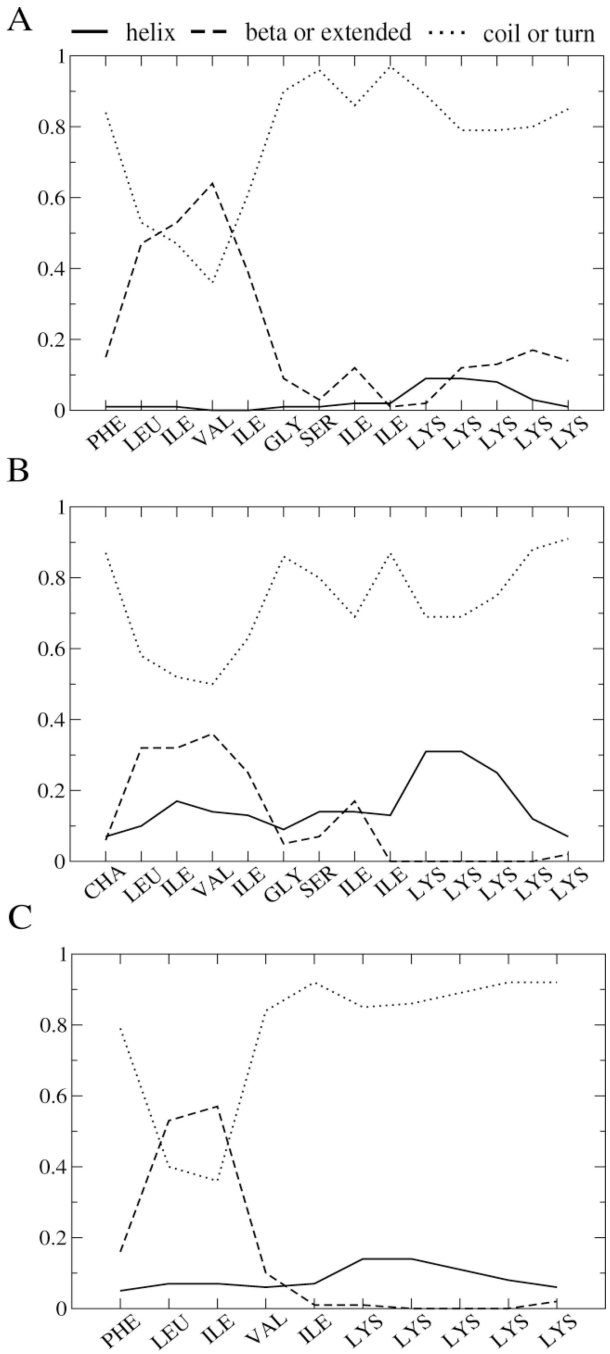

Figure 5.

Secondary structures of BAPs in the bilayer. A: bis(Ac-FLIVIGSII)-K-K_4-CO-NH_2; B: bis(Ac-CHA-LIVIGSII)-K-K_{4v} and C: bis(Ac-FLIVI)-K-K_4-CO-NH_2. Data were collected from last 400 ns of simulations and averaged over both branched hydrophobic segments.

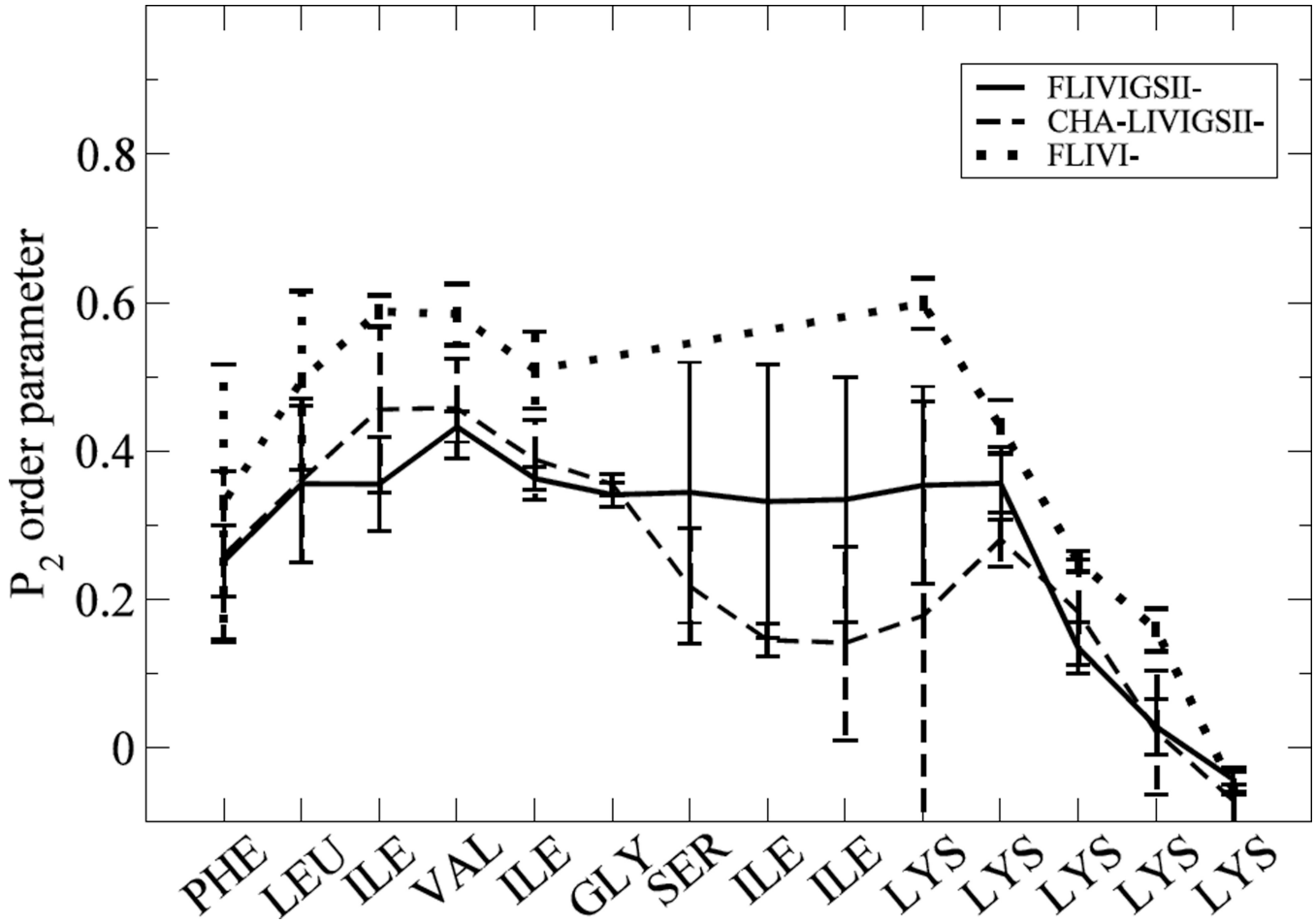

Figure 6.

P_2 order parameter as a function of the sequence. Data were collected from last 400 ns of simulations and were averaged over both tails. The error bars were calculated as the standard deviations from the three independent runs performed for each BAP.

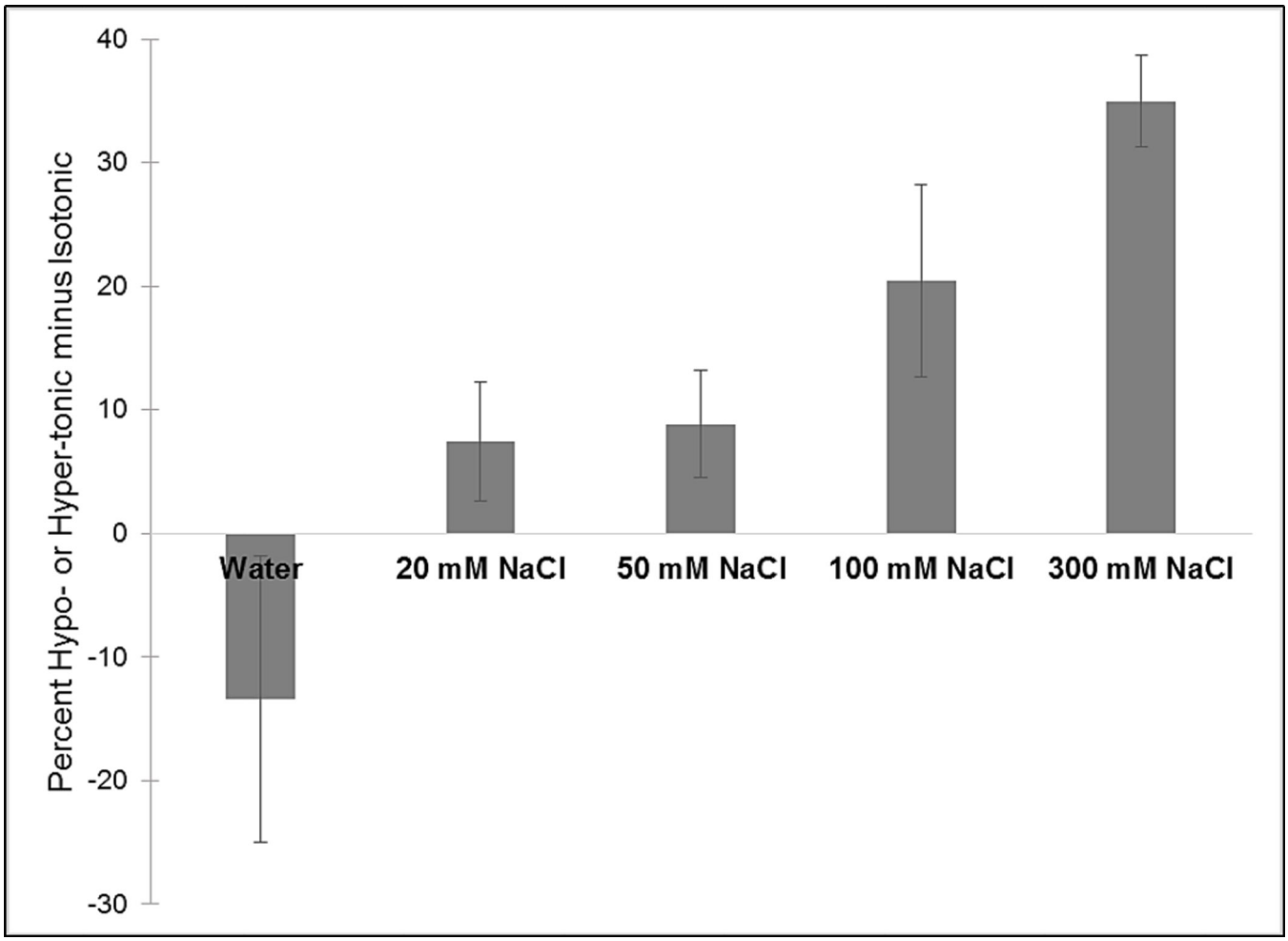

Figure 7.

Intensity differences between the percent fluorescence seen of Eosin Y dye encapsulated within BAPCs made in increasing concentrations of salt. The horizontal axis labels show the salt concentration, which was encapsulated within the BAPCs along with the Eosin Y dye. The vertical axis represents the difference in percent between the fluorescence seen in hyper- or hypo-tonic solutions minus that fluorescence seen in isotonic solutions. Error bars represent standard deviations with n≥3.

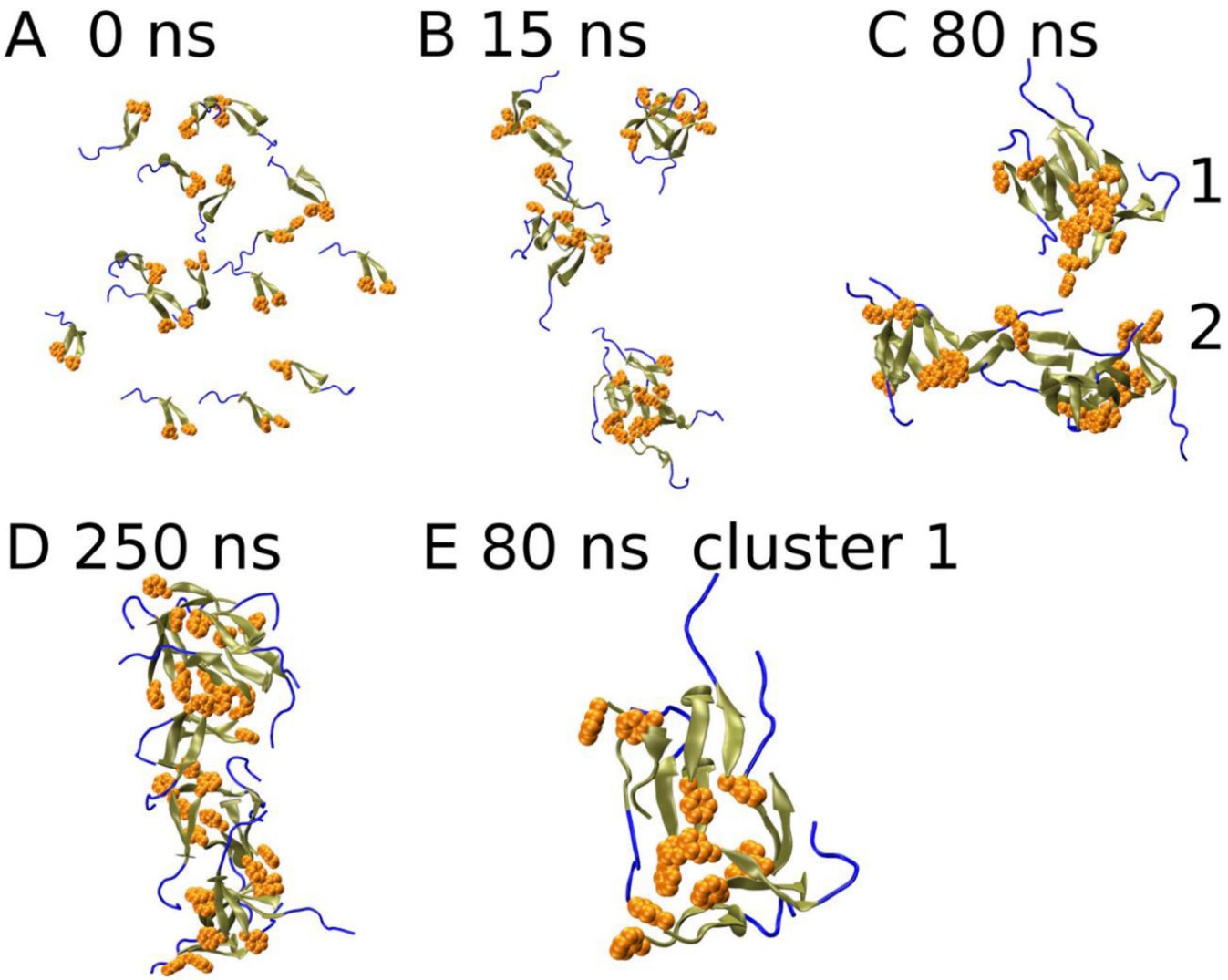

Figure 8.

Snapshots from early stages of BAP aggregation and self-assembly at A) 0 ns; B) 15 ns; C) 80 ns, and D) 250 ns. Panel E) provides a close-up view of cluster 1 at 80 ns (see Panel C). BAP molecules are shown in cartoon representations and colored according to residue types (positive: blue; hydrophilic: green; hydrophobic: brown). PHE1 residues are represented using van der Waals surfaces and colored in orange.

Table 1

Summary of the simulation systems.

Hydrophobic Segment	**bis(Ac-FLIVIGSII)-**	**bis(Ac-CHA-LIVIGSII)-**	**bis(Ac-FLIVI)-**	**bis(Ac-FLIVI)-**
Initial configuration	bilayer	bilayer	bilayer	dispersed
Initial box size (nm)	9.6×9.6×13.0	9.6×9.6×13.0	9.6×9.6×11.0	10.0×10.0×10.0
No. of atoms	~93,000	~93,000	~71,000	~97,000
Simulation length (μs)[a]	1.1, 0. 96, 0.68	1.0, 0. 64, 0.70	1.0, 0.87, 0.96	0.25

[a]Each independent simulation was initiated from a different bilayer configuration.

Table 2

Key structural and dynamic properties of BAP bilayers[a].

Hydrophobic Segment	bis(Ac-FLIVIGSII)-	bis(Ac-CHA-LIVIGSII)-	bis(Ac-FLIVI)-
Area per peptide(nm^2)	1.46±0.13	1.51±0.07	1.30±0.03
R_g(z) (nm)	0.63±0.03	0.61±0.04	0.53±0.01
Packing density[b]	0.85	0.78	0.68
S of PHE sidechains	0.004±0.001	N/A	0.02±0.01
# of inter-molecular hydrogen bonds[c]	4.3±0.3	4.0±0.2	3.3±0.5
# of intra-molecular hydrogen bonds[c]	6.7±0.8	6.5±0.8	4.4±0.1
# of BAP-water hydrogen bonds	9.7±1.3	10.0±1.1	3.2±0.5
Inter-molecular hydrogen bond lifetime (ps)	57.3±20.0	55.7±17.0	70.4±29.9
Intra-molecular hydrogen bond lifetime (ps)	53.2±18.2	33.7±11.4	70.2±41.2
# of Cross-leaflets hydrogen bonds	1.4±0.1	1.8±0.1	0.7±0.3
Lowest water electron density ($e.nm^{-3}$)	5.2±1.8	4.0±1.0	3.7±1.4
Water conduct rate ($nm^{-1}.ns^{-1}$)	0.03±0.02	0.03±0.01	0.06±0.01
Average time for single water molecule cross the bilayer core (ns)	14±6	17±4	9±1
Peptide lateral diffusion coefficient ($10^{-10}cm^2/s$)	2.1 ± 1.0	2.5 ± 0.7	2.3 ± 0.2

[a] All standard deviations shown were calculated from three independent runs performed for each BAP.

[b] The packing density is defined as $\pi * R_g(z)^2/A$, where A is the average area per peptide.

[c] Only hydrogen bond formed between hydrophobic segment were counted.